



RESEARCH ARTICLE

Abnormal dynamic functional connectivity is linked to recovery after acute ischemic stroke

Anna K. Bonkhoff^{1,2}  | Markus D. Schirmer^{1,3} | Martin Bretzner^{1,4} | Mark Etherton¹ | Kathleen Donahue¹ | Carissa Tuozzo¹ | Marco Nardin¹ | Anne-Katrin Giese^{1,5} | Ona Wu⁶ | Vince D. Calhoun⁷ | Christian Grefkes^{2,8}  | Natalia S. Rost¹

¹J. Philip Kistler Stroke Research Center, Massachusetts General Hospital, Boston, Massachusetts

²Cognitive Neuroscience, Institute of Neuroscience and Medicine (INM-3), Research Centre Juelich, Juelich, Germany

³Department of Population Health Sciences, German Centre for Neurodegenerative Diseases (DZNE), Germany

⁴Neurosciences and Cognition, University of Lille, Lille, France

⁵Department of Neurology, University Medical Center Hamburg-Eppendorf, Hamburg, Germany

⁶Athinoula A. Martinos Center for Biomedical Imaging, Department of Radiology, Massachusetts General Hospital, Charlestown, Massachusetts

⁷Tri-institutional Center for Translational Research in Neuroimaging and Data Science (TReNDS), Georgia State University, Georgia Institute of Technology, Emory University, Atlanta, Georgia

⁸Department of Neurology, University Hospital Cologne, Cologne, Germany

Correspondence

Anna K. Bonkhoff, J. Philip Kistler Stroke Research Center, Massachusetts General Hospital, 175 Cambridge Street, Suite # 300, Boston, MA 02114.
Email: abonkhoff@mgh.harvard.edu

Funding information

Deutsche Forschungsgemeinschaft, Grant/Award Number: Project-ID 431549029; National Institutes of Health, Grant/Award Number: R01DA040487; NIH-NINDS, Grant/Award Numbers: R01NS082285, R01NS086905, U19NS115388

Abstract

The aim of the current study was to explore the whole-brain dynamic functional connectivity patterns in acute ischemic stroke (AIS) patients and their relation to short and long-term stroke severity. We investigated resting-state functional MRI-based dynamic functional connectivity of 41 AIS patients two to five days after symptom onset. Re-occurring dynamic connectivity configurations were obtained using a sliding window approach and k-means clustering. We evaluated differences in dynamic patterns between three NIHSS-stroke severity defined groups (mildly, moderately, and severely affected patients). Furthermore, we built Bayesian hierarchical models to evaluate the predictive capacity of dynamic connectivity and examine the interrelation with clinical measures, such as white matter hyperintensity lesions. Finally, we established correlation analyses between dynamic connectivity and AIS severity as well as 90-day neurological recovery (Δ NIHSS). We identified three distinct dynamic connectivity configurations acutely post-stroke. More severely affected patients spent significantly more time in a configuration that was characterized by particularly strong connectivity and isolated processing of functional brain domains (three-level ANOVA: $p < .05$, post hoc t tests: $p < .05$, FDR-corrected). Configuration-specific time estimates possessed predictive capacity of stroke severity in addition to the one of clinical measures. Recovery, as indexed by the realized change of the NIHSS over time, was significantly linked to the dynamic connectivity between bilateral intraparietal lobule and left angular gyrus (Pearson's $r = -.68$, $p = .003$, FDR-corrected). Our findings demonstrate transiently increased isolated information processing in multiple functional domains in case of severe AIS. Dynamic connectivity involving default mode network components significantly correlated with recovery in the first 3 months poststroke.

KEYWORDS

Bayesian hierarchical modeling, dynamic functional network connectivity, ischemic stroke, stroke recovery, stroke severity

1 | INTRODUCTION

One in four adults over the age of 25 experiences a stroke during their lifetime (Collaborators, 2018) and is thus frequently confronted with multifaceted long-term impairments (Corbetta et al., 2015). Establishing a comprehensive understanding of cerebral changes early after stroke is of prime importance to successfully design rehabilitative strategies. In this respect, functional neuroimaging has proven to be instrumental in uncovering neural mechanisms of reorganization poststroke (Grefkes & Fink, 2014; Ward, 2017). Motor impairments have previously been linked to decreases in functional connectivity between sensorimotor areas across hemispheres (Carter et al., 2010; Rehme et al., 2014). Post-stroke cognitive impairments and affective symptoms have been associated with functional connectivity alterations in default mode network regions (Ding et al., 2014; Lassalle-Lagadec et al., 2012).

Conventional resting-state functional MRI (rsfMRI) analyses typically evaluate functional connectivity over the duration of entire scan sessions (i.e., several minutes). Contrariwise, recently developed time-varying—dynamic—functional network connectivity (dFNC) analyses allow moment-to-moment connectivity strengths fluctuations and, by these means, enable a time-resolution in the order of seconds (Allen et al., 2014; Calhoun, Miller, Pearlson, & Adalı, 2014; Chang & Glover, 2010). Numerous studies suggest that this dynamic approach represents a powerful tool to gain novel insights into neurological diseases, for example, migraine (Tu et al., 2019), Parkinson's disease (Kim et al., 2017) and Huntington's disease (Espinoza et al., 2018). In case of ischemic stroke, the dFNC analysis has been essential in revealing transiently increased information exchange between motor domains in moderate motor stroke and more isolated information processing in severe motor stroke (Bonkhoff et al., 2020).

In extension to previous dFNC analyses in acute ischemic stroke (AIS), we here investigated dynamic connectivity not only between motor regions, but regions covering the whole brain of 41 AIS patients. Additionally, we evaluated links to acute stroke severity, as well as recovery. We hypothesized that large-scale, transient alterations in information processing were driven by AIS severity and featured predictive capacity.

2 | MATERIALS AND METHODS

2.1 | Participants

We considered rsfMRI scans from 47 AIS patients who were admitted to Massachusetts General Hospital, USA and subsequently enrolled in the SALVO (statins augment small vessel function and improve stroke outcomes) study between 2014 and 2019. The following SALVO-specific inclusion criteria were applied: (a) admission ≤ 24 hours from onset of focal neurological symptoms consistent with a cerebrovascular syndrome, (b) MRI findings corresponding to acute cerebral ischemic injury (e.g., DWI-positive lesions), and (c) evidence of moderate to severe WMH lesion load (Fazekas grade ≥ 2 , Fazekas, Chawluk, Alavi, Hurtig, & Zimmerman, 1987). Exclusion criteria included: (a) the primary

hemorrhagic stroke or evidence of secondary cause of stroke (e.g., primary central nervous system vasculitis, auto-immune encephalitis, known malignancy), (b) medical contraindications to MRI or gadolinium-based contrast agents, (c) severe medical or behavioral co-morbidities and (d) pregnancy or lactation at the time of screening. Language impairments and neglect did not lead to study exclusion. One stroke patient had to be excluded due to structural abnormalities (benign brain cyst) and five further participants due to pronounced head motion during image acquisition (maximum framewise translation: >3 mm, maximum framewise rotation >0.05 rad). Therefore, 41 subjects were included in the analyses. The study was approved by the institutional review board (Massachusetts General Hospital) and all participants, or their surrogates, gave written informed consent at the time of enrollment.

2.2 | Clinical assessment

Individual stroke severity, quantified by means of the National Institutes of Health Stroke Scale score (NIHSS), was obtained by trained neurologists at multiple instances post-stroke (admission, time of the rsfMRI scan, 90 day). We defined three groups of stroke patients based on NIHSS scores at time of scanning: mildly affected (NIHSS: 0–2, $n = 19$), moderately affected (NIHSS: 3–9, $n = 15$), and severely affected (NIHSS 10–21, $n = 7$). Cutoffs were chosen based on the sample-specific distribution of NIHSS scores (Table S1) with the aim of creating as homogeneous groups with regard to stroke severity as possible. In view of the less frequent recruitment of severely affected patients and resulting group imbalance, we additionally performed correlation and regression analyses to augment group-dependent with group-independent results. Patient groups were compared with respect to their white matter hyperintensity (WMH) lesion volume and maximum framewise displacement (one-way three-level ANOVAs, Power, Schlaggar, & Petersen, 2015).

2.3 | Data acquisition

Patients were scanned at admission (DWI, 1.5 T, General Electric scanner) as well as 2 to 5 days after stroke onset (functional scans, 3.0 T, Siemens Skyra scanner). We here relied on diffusion weighted images (DWI) and rsfMRI data with the following parameters: DWI: echo-planar imaging, number of slices: 28; slice thickness: 5 mm; repetition time (TR): 5500 ms; echo time (TE): 99 ms; in-plane resolution: 1.375 mm, and rsfMRI (~6 mins): gradient-echo planar imaging (EPI) sequence, 150 volumes, number of slices: 42 (interleaved); slice thickness: 3.51 mm; matrix size: 64×64 ; flip angle: 90° ; repetition time (TR): 2400 ms; in-plane resolution: 3.437 mm.

2.4 | Preprocessing of rsfMRI data

Preprocessing of the rsfMRI data was conducted using MATLAB (Version R2019b, MathWorks, Inc., Natick, MA) and the Statistical

Parametric Mapping software package (SPM12, Wellcome Trust Centre for Neuroimaging, London, UK; www.fil.ion.ucl.ac.uk/spm). After removal of the first three images ("dummy images") to ensure a steady BOLD-signal, the remaining 147 volumes were head movement-corrected through affine realignment to each scan's mean image. Diffusion-weighted images, as well as corresponding lesion masks were linearly co-registered to the same functional mean image (c.f., lesion overlap, Figure S1). All volumes were then non-linearly spatially normalized employing the "unified segmentation" option with masked lesions (i.e., setting lesioned tissue areas to values of zero to reduce lesion-caused spatial distortions during the normalization step, Ashburner & Friston, 2005; Brett, Leff, Rorden, & Ashburner, 2001). Finally, images were smoothed using a Gaussian kernel with a full-width at half maximum (FWHM) of 8 mm. For each patient, we estimated the maximum time lag between time courses of the left and right hemisphere (c.f., Supplementary Materials, *Time delay analysis*).

2.5 | Intrinsic connectivity networks

We used the spatially constrained independent component analysis (ICA) algorithm (Du & Fan, 2013; Salman et al., 2019) to back-reconstruct individual spatial information and time-courses of 50 ICA components (as available from Allen et al., 2014). We relied on previously estimated ICA components, originating from the analysis of data from healthy subjects (Allen et al., 2014) to avoid any potential lesion-induced spatial biases. One component (caudate) did not pass quality control after back-reconstruction (spatial inaccuracies) and was therefore excluded. The remaining 49 components were organized into seven functional domains: (a) sensorimotor, (b) subcortical, (c) cerebellar, (d) visual, (e) auditory, (f) cognitive control, and (g) default mode network (Figure 1). Additional postprocessing steps were applied: We detrended (i.e., accounted for linear, quadratic and cubic trends), despiked using 3Ddespike, and filtered time courses by a fifth-order Butterworth low-pass filter with a high-frequency cutoff of 0.15 Hz. Lastly, each time-course was variance-normalized.

2.6 | Dynamic functional network connectivity

DFNC was computed within the sliding window framework (Allen et al., 2014; Calhoun et al., 2014; Damaraju et al., 2014). As in previous studies (Allen et al., 2014; Bonkhoff, Espinoza, et al., 2020), the width of the window was chosen to be close to 44 s (18 TRs). Time windows were additionally convolved with a Gaussian of 7 s (3 TRs) and shifted at a rate of 1 TR at a time. Therefore, we obtained 129 tapered time windows per subject. Dynamic connectivity between the various networks for each time window was computed via the l_1 -regularized precision matrix (Varoquaux, Gramfort, Poline, & Thirion, 2010). We regressed out the covariates age, sex, maximum framewise translation, and rotation to decrease differences between patients. Finally, connectivity values were Fisher Z-transformed.

2.7 | Estimation of connectivity states

We utilized k-means clustering (l_1 distance, Lloyd, 1982) to reveal latent dynamic functional connectivity configurations, that is, *connectivity states*. These states represented repeating connectivity patterns across time and subjects (Allen et al., 2014; Calhoun et al., 2014). The clustering procedure was conducted in a two-step procedure: We first derived the optimal number of clusters k (=number of connectivity states) in an initial run. The optimal number k was defined based on commonly used criteria in previous dFNC studies: The elbow criterion resting upon the cluster validity index (Allen et al., 2014) and a state frequency of >10% (Espinoza et al., 2019). Secondly, we computed the final k connectivity states. For every subject, each time window was assigned to one of the k connectivity states. In a final step, we computed the following dFNC specific measures: (a) *fraction times* (the subject-specific fraction of total time spent in a state), (b) *dwell times* (the subject-specific average time spent in a state without interruption) and (c) *state transitions* (the subject-specific number of changes between states over the duration of the scan). Additionally, we obtained subject- and state-specific dFNC strength matrices.

2.8 | Statistical analysis

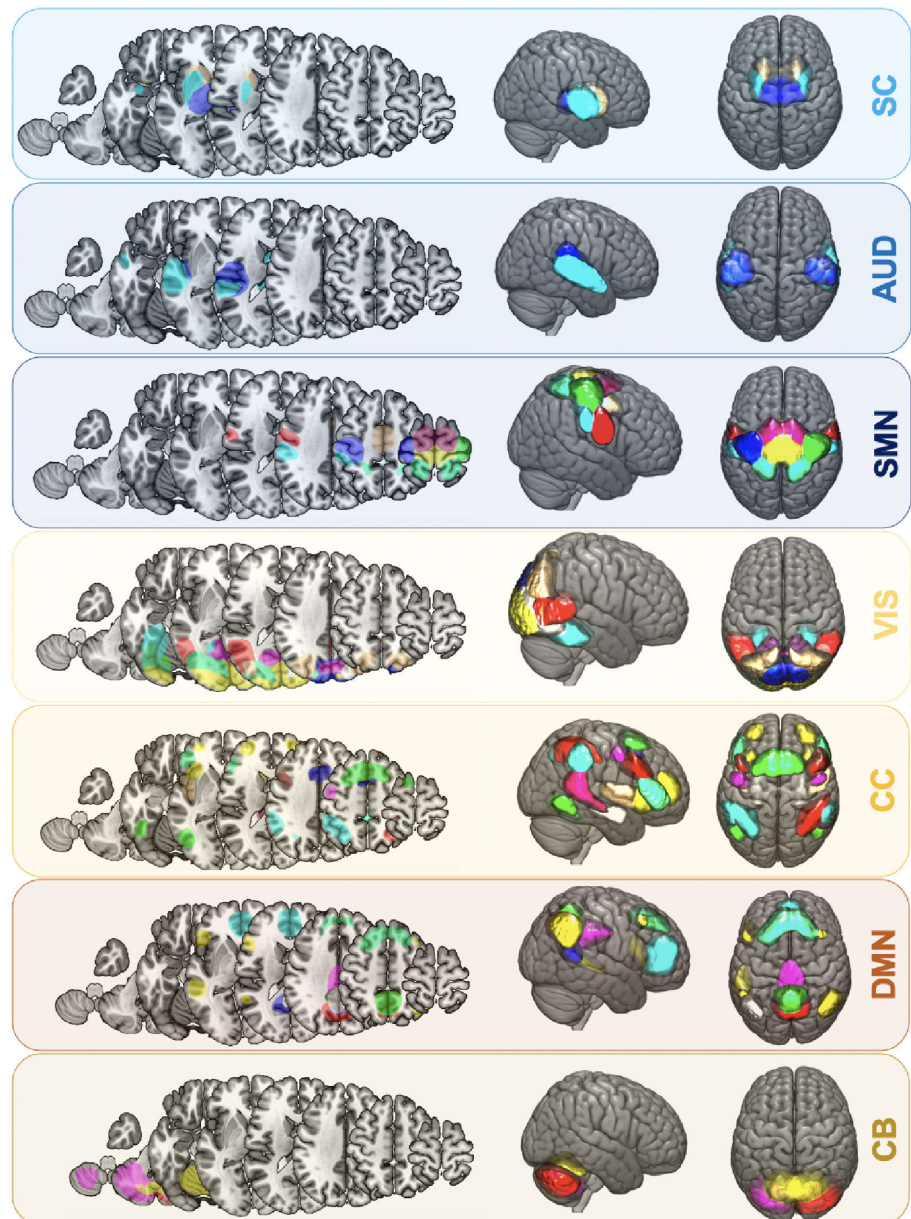
2.8.1 | Group differences

Differences in dynamic patterns (fraction and dwell times, transitions, dFNC strengths) with respect to group membership and thus stroke severity were determined in three-level one-way ANOVAs (level: mildly vs. moderately vs. severely affected patients, level of significance, $p \leq .05$). In case of significant ANOVA effects, we followed up with post hoc t tests between the individual groups (mild vs. moderate, mild vs. severe, moderate vs. severe; level of significance, $p \leq .05$, False discovery rate [FDR]-corrected). We then conducted correlation analyses between significant dFNC measures and NIHSS_{scan} pairs (Pearson correlation, level of significance, $p \leq .05$, FDR-corrected). We furthermore ran partial correlation analyses between the significant dFNC measures and NIHSS-based recovery. We captured recovery as realized recovery potential: $(\text{NIHSS}_{90\text{days}} - \text{NIHSS}_{\text{scan}}) / (0 - \text{NIHSS}_{\text{scan}})$ (Pearson correlation, level of significance, $p < .05$, FDR-corrected, adjusted for NIHSS_{scan}, c.f., Lin et al., 2019). Given the inclusion criterion of a higher WMH lesion load, we performed further correlation analyses between dFNC measures and the WMH lesion load (Pearson correlation, level of significance, $p \leq .05$, FDR-corrected).

2.8.2 | Bayesian prediction of AIS severity

We constructed linear regression models to test the capacity of clinical and dynamic connectivity derived variables to predict stroke severity at time of the scan. We employed Bayesian hierarchical models, primarily as these models allow for (a) a full estimation of parameter

FIGURE 1 Spatial maps of 49 intrinsic connectivity networks of all ischemic stroke subjects ($n = 41$). Networks were assigned to seven functional domains: Subcortical (SC, 3 networks, *light blue*), auditory (AUD, 3 networks, *blue*), cortical sensorimotor (SMN, 8 networks, *dark blue*), visual (VIS, 10 networks, *yellow*), cognitive control (CC, 14 networks, *orange*), default mode network (DMN, 9 networks, *brown*), cerebellar domain (CB, 3 networks, *moccasin*)



uncertainty, (b) an intuitive interpretation of credibility intervals, and (c) Bayesian model comparisons (Gelman & Hill, 2006). Furthermore, given the inclusion criterion of a pronounced WMH load, the hierarchical nature of models permitted to investigate differential effects of moderate versus high loads of WMH lesions on stroke severity. The two groups of WMH load were integrated as a varying intercept. Therefore, we initiated one intercept for the moderate and one for the high WMH lesion load group. Both of these intercepts were combined by a joint hyperprior. We then built individual models relying on either admission NIHSS (the acute baseline model, c.f., Ktena et al., 2019) or dFNC measures (dwell times for State 1–3, the acute dynamic model). We did not integrate fraction times and numbers of transitions in addition to dwell times to reduce probable collinearity of input variables. Subsequently, we combined all of these input variables for an extended model of acute stroke severity (the acute

extended model). A final Bayesian model comparison based on leave-one-out-cross-validation (LOOCV) was performed to determine the most suitable among the three models to predict stroke severity of future patients. In ancillary analyses, we evaluated the effects of further covariates, that is, age, sex and the administration of intravenous thrombolysis.

2.9 | Data and code availability statement

The authors agree to make the data available to any researcher for the express purposes of reproducing the here presented results and with the explicit permission for data sharing by the local institutional review board. Preprocessing of data and dFNC were computed in Matlab2019a (The Mathworks, Natick, MA) and used adjusted

template scripts from the GIFT toolbox (<https://trendscenter.org/software/gift/>). Additional computations were run in Python3.7, particularly relying on the package pymc3 (Salvatier, Wiecki, & Fonnesbeck, 2016) and rapidtide (Erdoğan, Tong, Hocke, Lindsey, & deB Frederick, 2016). Relevant jupyter notebooks can be found here: https://github.com/AnnaBonkhoff/DFNC_AIS_recovery.

3 | RESULTS

3.1 | Clinical characteristics

Forty-one included AIS patients were scanned upon admission and 2 to 5 days after stroke onset. Stroke severity was captured at several time instances, median NIHSS_{admission} was 4 (interquartile range [IQR] = 10, 40 patients), median NIHSS_{scan}: 3 (IQR = 4, 41 patients) and median NIHSS_{90days}: 0 (IQR = 1, 29 patients with follow-up-data). Neither one of our stroke patients featured a hemispheric delay of more than a second. Further demographical and clinical characteristics are displayed in Table 1.

3.2 | Dynamic functional network connectivity

After the back-reconstruction of spatial maps and time courses of 49 networks originating from seven functional domains, we computed and explored characteristics of *dynamic* functional connectivity. Importantly, we regressed out effects of age, sex, and motion at this point. The cluster validity index indicated three clusters as the optimal

TABLE 1 Demographics and clinical characteristics of AIS patients undergoing rsfMRI

	Acute: stroke patients (n = 41)	90 days: stroke patients (n = 29)
Age (years, mean, SD)	67.3 (9.9)	66.9 (10.0)
Sex (in % female)	32%	27%
NIHSS _{admission} (median, IQR)	4 (10)	4 (9)
NIHSS _{scan} (median, IQR)	3 (4)	2 (2)
NIHSS _{90days} (median, IQR)	–	0 (1)
Intravenous thrombolysis	34%	35%
Mechanical thrombectomy	2%	4%
Normalized lesion volume (ml, mean, SD)	14.0 (21.1)	8.8 (13.7)
Vascular risk factors		
Hypertension	70.7%	72.4%
Diabetes mellitus	19.5%	10.3%
Atrial fibrillation	26.8%	20.7%
Previous myocardial infarction	17.1%	20.7%
Current smoker	19.5%	20.7%
Previous smoker	41.5%	41.4%

solution. Thus, each subject's 129 functional connectivity matrices were assigned to one of three connectivity states (Figure 2).

State 1 was the most segregated state and also appeared the least often (overall frequency: 21%, Figure 2, *left panel*). It featured highly positive intra-domain connectivity. Highly negative inter-domain connectivity emerged between the cortical sensorimotor and the cerebellar as well as the visual domains. State 2, the most frequent connectivity state, displayed a markedly different connectivity pattern: It was characterized by mostly neutral inter-domain and only slightly positive intra-domain connectivity (frequency: 54%, Figure 2, *middle panel*). State 3, occurring with a frequency of 25%, displayed highly positive intra-domain connectivity in the sensorimotor and visual domains, resembling State 1 in this respect, but also positive inter-domain connectivity between these two domains (Figure 2, *right panel*).

3.3 | Temporal characteristics

Next, we evaluated differences in dynamic patterns between the three groups of patients (mild: 0–2 vs. moderate: 3–9 vs. severe: 10–21 NIHSS). By means of three-level one-way ANOVAs, we detected significant differences of dynamic patterns relating to State 1, the state with the highest functional segregation (Fraction times: $p = .01$; dwell times: $p = .002$, Figure 3). While mildly and moderately affected patients did not differ based on post hoc t tests, we found significantly different fraction times between mildly and severely affected patients as well as significantly different dwell times between mildly and severely as well as moderately and severely affected patients (Fraction times: mild–moderate: $p = .51$, mild–severe: $p = .01$, moderate–severe: $p = .08$, FDR-corrected; dwell times: mild–moderate: $p = .82$, mild–severe: $p = .01$, moderate–severe: $p = .03$, FDR-corrected). Severely affected patients generally spent more time in State 1. These significant differences between discrete groups were also found in continuous Pearson correlations: NIHSS_{scan} significantly correlated with fraction, as well as dwell times of State 1 (Fraction time and NIHSS: $r = .49$, $p = .001$, dwell time and NIHSS: $r = .55$, $p < .001$). This, once again, demonstrated that more profound symptom severity increased the amount of time spent in the highly segregated State 1. The number of state transitions did not differ significantly between the three groups of variably affected patients (three-level one-way analysis of variance [ANOVA]: $p = .40$). We did not observe any significant correlations between any of the fraction or dwell times and recovery in stroke severity, or the WMH lesion load ($p > .05$). The three groups of patients did not significantly differ with respect to their WMH lesion load (mean [SD]: mild: 21.36 (29.5) ml, moderate: 13.1 (15.7), severe: 15.6 (15.8), $p = .58$) and the maximum framewise displacement (mean [SD]: mild: 1.1 (0.6), moderate: 1.0 (0.6), severe: 1.6 (0.4), $p = .07$).

3.4 | Alterations in dynamic connectivity

Focusing on the differences in dFNC strengths, we identified numerous connectivity state-specific group differences (one-way ANOVA:

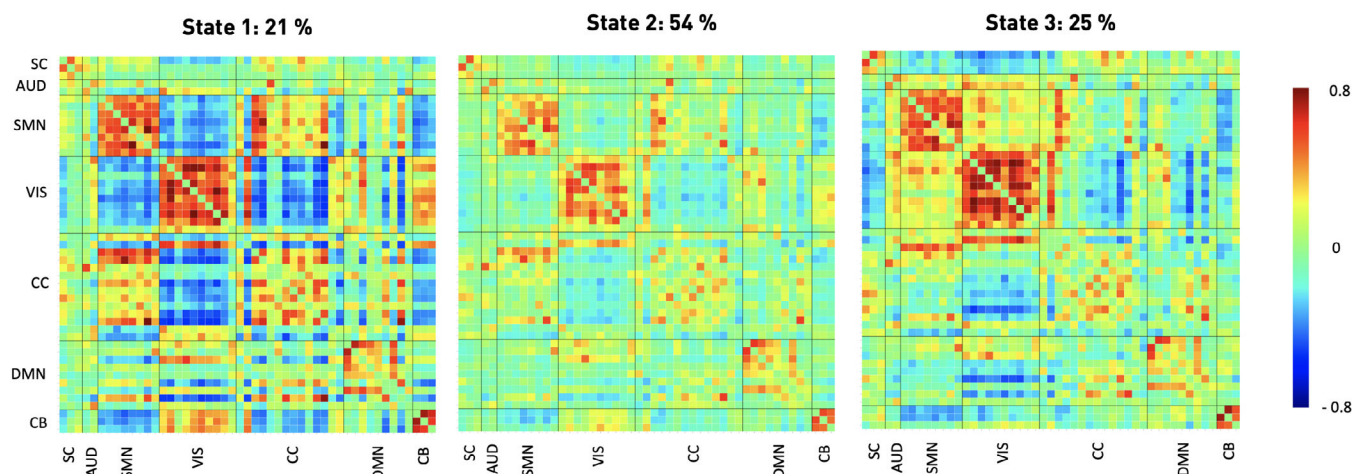


FIGURE 2 Three discrete connectivity states representing re-occurring dynamic connectivity across time and subject space. These states demonstrated varying connectivity configurations between seven functional domains (c.f., Figure 1). Darker red color implies stronger positive, darker blue stronger negative connectivity. Stated percentages correspond to state-specific fraction times across all subjects. The ordering of states corresponds to the one introduced by the k-means algorithm

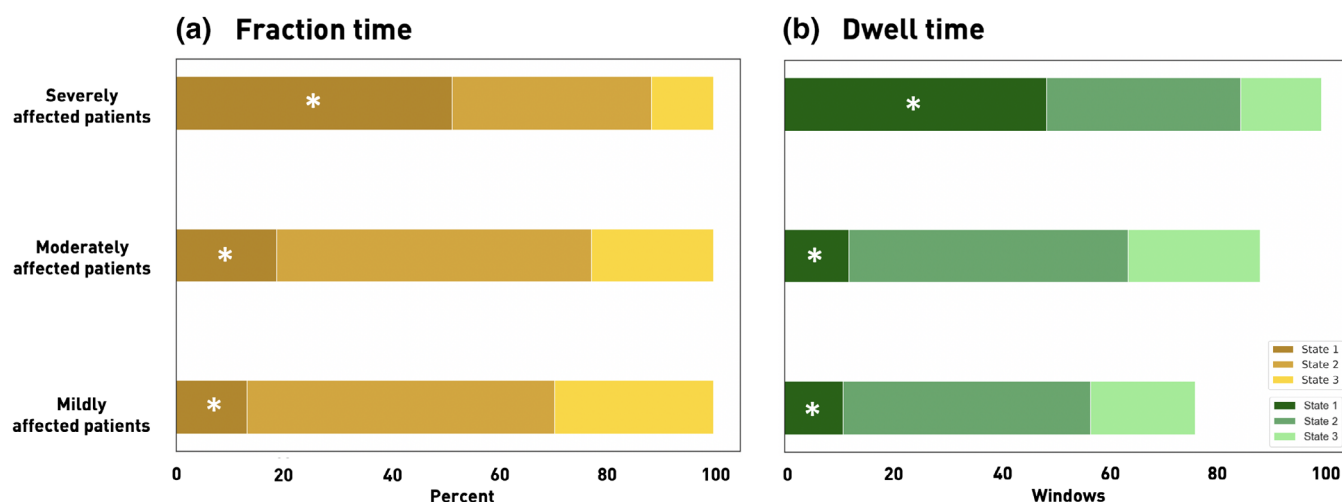


FIGURE 3 Fraction and dwell times for each of the three dynamic connectivity states and stroke severity defined subgroups of mildly, moderately and severely affected patients (asterisks mark statistically significant differences between patient subgroups based on one-way ANOVAs, $p < .05$). (a) Fraction times. Severely affected patients (NIHSS >9 , upper row) presented with a markedly different dynamic pattern than moderately (NIHSS 3–9, middle row) and mildly (NIHSS <3 , bottom row) affected patients: In contrast to the other two patient groups that preferred State 2, a particularly weakly connected state, severely affected patients spent significantly more time in the densely connected State 1. (b) Dwell times. In parallel to the fraction time findings, severely affected patients spent significantly more time in State 1 at any one time in comparison to the less affected patient groups

$p \leq .05$). The densely connected State 1 contained most of these differences. Specifically, post hoc t tests between mildly and moderately affected patients for example revealed decreased dynamic connectivity between bilateral precentral areas and the left sensorimotor area ($p \leq .05$, FDR-corrected, Figure 4, left panel). Mildly and severely affected patients comprised numerous significantly varying connectivity pairs (post hoc t tests: $p \leq .05$, FDR-corrected, c.f., Figure 4 for details, middle panel). These differences particularly involved connections between the bilateral superior temporal gyri and multiple cortical sensorimotor areas. Dynamic connectivity differences between

moderately and severely affected patients predominantly pertained to bilateral subcortical, superior temporal gyri and ventral precentral networks (post hoc t tests: $p \leq .05$, FDR-corrected, Figure 4, right panel). State 2, the weakly connected state, encompassed only two dynamic connectivity pairs that were significantly different between patient groups after FDR-correction: Mildly and severely affected patients differed in their dynamic connectivity between the right intraparietal lobule and middle occipital gyrus. Severely affected patients presented with an increased connectivity between bilateral superior parietal lobules and middle temporal gyri in contrast to moderately affected

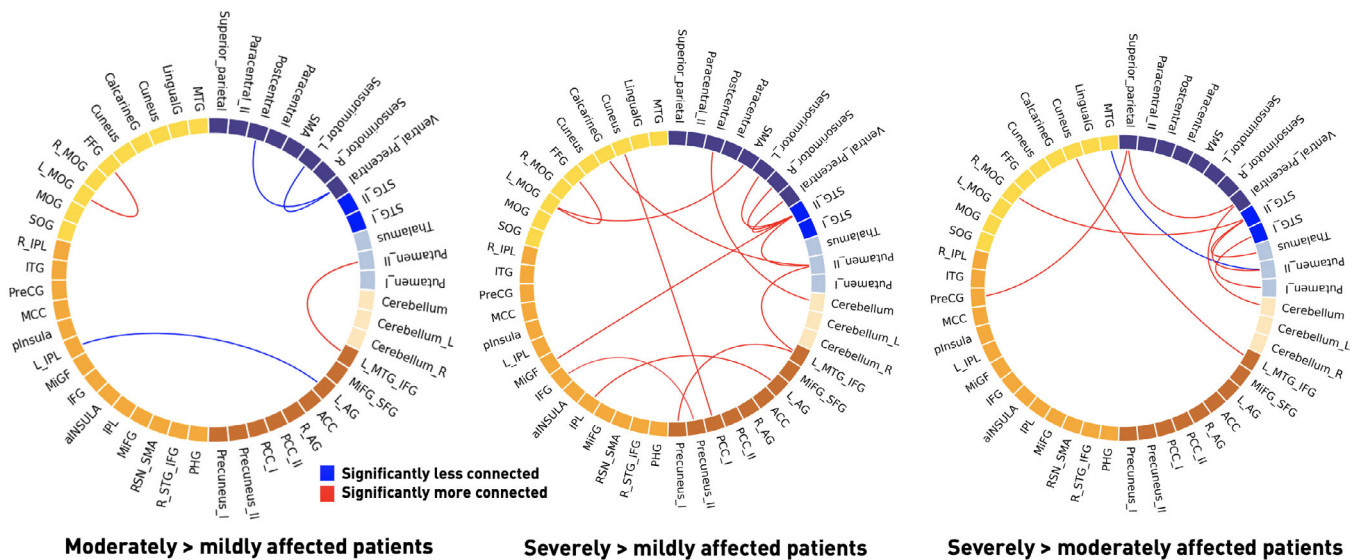


FIGURE 4 Significant dynamic connectivity differences between mildly, moderately and severely affected patient groups in State 1 (one-way ANOVAs: $p < .05$, post hoc t tests: $p < .05$, FDR-corrected). The functionally segregated state 1 comprised the most significantly altered connectivity pairs. Severely affected patients comprised numerous dynamic connectivity pairs with enhanced connectivity compared with both mildly and moderately affected patients. These changes primarily involved subcortical and cortical motor networks, as well as multiple connections to the default mode network

patients (Figure S2). State 3 was characterized by increased dynamic connectivity between the bilateral posterior insula and precuneus as well as decreased dynamic connectivity between a bilateral putamen network and anterior insula when contrasting moderately with mildly affected patients. A decreased dynamic connectivity between the lingual gyrus and right middle occipital gyrus was found when comparing severely to mildly affected patients (Figure S3). Altogether, most of these reported dynamic connectivity pairs were also significantly correlated with the $\text{NIHSS}_{\text{scan}}$ (Figure S4). However, such a significant correlation with the $\text{NIHSS}_{\text{scan}}$ was missing for the lateralized dynamic connectivity decrease between cortical motor networks.

In a subsequent step, we investigated whether the dynamic connectivity pairs that differed significantly between the groups also correlated with the realized recovery. We extracted two such connectivity pairs with significant correlations: In State 1, the connectivity of the bilateral intraparietal lobules and left angular gyrus was significantly correlated with change in stroke severity ($r = -.68$, $p = .003$, FDR-corrected, Figure 5a, upper plot, Figure 5b,c, upper row). Furthermore, the dynamic connectivity between the bilateral putamen network and the anterior insula within State 3 correlated strongly with stroke recovery ($r = .66$, $p = .05$, FDR-corrected, Figure 5a, bottom plot, Figure 5b,c, lower row). One further connectivity pair, featuring the bilateral putamen network and superior temporal gyri (STG), significantly correlated with recovery before the correction for multiple comparisons ($r = .61$, $p = .007$, uncorrected, $p = .08$, FDR-corrected, Figure 5a, bottom plot, Figure 5b,c, middle row), which may motivate more focused further investigation in future studies (Gibbs & Gibbs, 2015; Wood, Freemantle, King, & Nazareth, 2014). The effects of age, sex, and motion in the scanner were accounted for in the analyses reported above.

3.5 | Bayesian prediction of acute stroke severity

Bayesian hierarchical models, either taking $\text{NIHSS}_{\text{admission}}$ or the three dwell times as input, achieved comparable levels of explained variance when predicting stroke severity at the time of scanning (posterior predictive check: R^2 -scores: 32.2 and 32.8%, respectively). The extended acute model combining $\text{NIHSS}_{\text{admission}}$ and dwell times increased explained variance to 62.1%. The leave-one-out-cross-validation-based Bayesian model comparison also suggested the extended acute model as the best performing model (LOOCV-estimated deviance $\pm \text{SE} = 224.1 \pm 11.9$). The further two models, considering either $\text{NIHSS}_{\text{admission}}$ or the dwell times, followed on par (Deviance $\pm \text{SE} = 242.7 \pm 6.6$ and 246.2 ± 10.3 , respectively). Interpreting parameter weights: A higher $\text{NIHSS}_{\text{admission}}$ score predicted a higher $\text{NIHSS}_{\text{scan}}$ (posterior mean = 0.51, highest probability density interval [HPDI] covering 94% uncertainty = 0.29–0.74, Figure 6a). The same was true for higher dwell times in State 1 and, to a lesser degree, to higher dwell times in State 2 and 3 (State 1: posterior mean = 0.124, HPDI = 0.063 to 0.182; State 2: posterior mean = 0.028, HPDI = -0.012 to 0.064; State 3: posterior mean = 0.028, HPDI = -0.023 to 0.080, Figure 6b). Varying intercepts for the groups of moderate and high white matter hyperintensity loads only diverged in case of the model including $\text{NIHSS}_{\text{admission}}$ only (moderate WMH load: posterior mean = -0.266, HPDI = -3.786 to 3.066, high WMH load: posterior mean = 1.441, HPDI = -0.659 to 3.667). Here, higher white matter hyperintensity load indicated a higher NIHSS outcome at the time of scanning. A similar divergence of intercepts was not visible in the acute dynamic or extended acute models. Ancillary analyses suggested a trend for higher stroke severities with increasing age, but did not suggest any

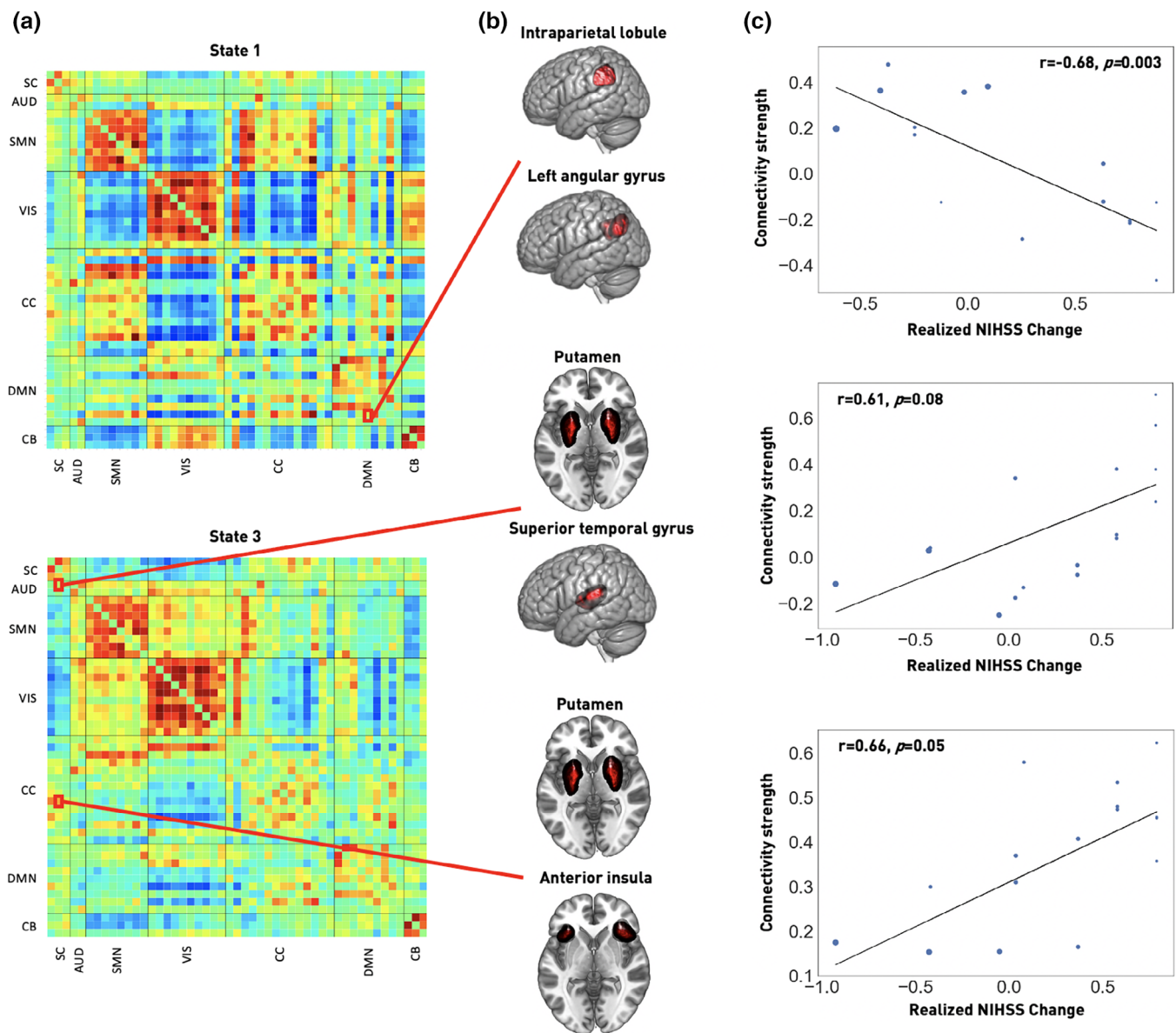


FIGURE 5 Recovery in the first 3 months after stroke is linked to specific acute dynamic connectivity pairs. (a) Recovery-correlated connectivity pairs are highlighted within dynamic connectivity State 1 (upper row) and State 3 (bottom row). These connectivity pairs were located in subcortical (SC), auditory (AUD), cognitive control (CC) and default mode network (DMN) domains. (b) Brain renderings of involved networks. In State 1, the connectivity between the bilateral intraparietal lobule and left angular gyrus was significantly correlated with recovery after correction for multiple comparison. In State 3, the connectivity between bilateral putamen and anterior insula was significantly correlated with recovery after correction for multiple comparisons, while the connectivity between bilateral putamen and superior temporal gyrus was significantly correlated with recovery before correction for multiple comparisons. These latter findings may motivate a re-examination in future studies. (c) Correlation plots. Recovery, measured as realized change in NIHSS and adjusted for $\text{NIHSS}_{\text{scan}}$, is plotted on the x-axis, dFNC strength on the y-axis (p-values are FDR-corrected). The size of the dots corresponds to an individual's stroke severity at time of scanning

additional effect of the administration of rtPA or sex on the stroke severity at time of scanning (R^2 -score = 64.9%).

4 | DISCUSSION

Dynamic functional network connectivity analyses permit the evaluation of brain connectivity alterations in the range of seconds (Allen

et al., 2014; Calhoun et al., 2014; Chang & Glover, 2010). This approach, therefore, may capture naturally fluctuating neural signals in a more veridical and behaviorally relevant way (Vidaurre, Arenas, Smith, & Woolrich, 2019). We here examined alterations of whole-brain dynamic connectivity in 41 AIS patients in relation to the severity of their acute stroke deficit. We identified three dynamic connectivity states, which were strongly related to the severity of symptoms. Most remarkably, severely affected stroke patients ($\text{NIHSS} > 9$) spent

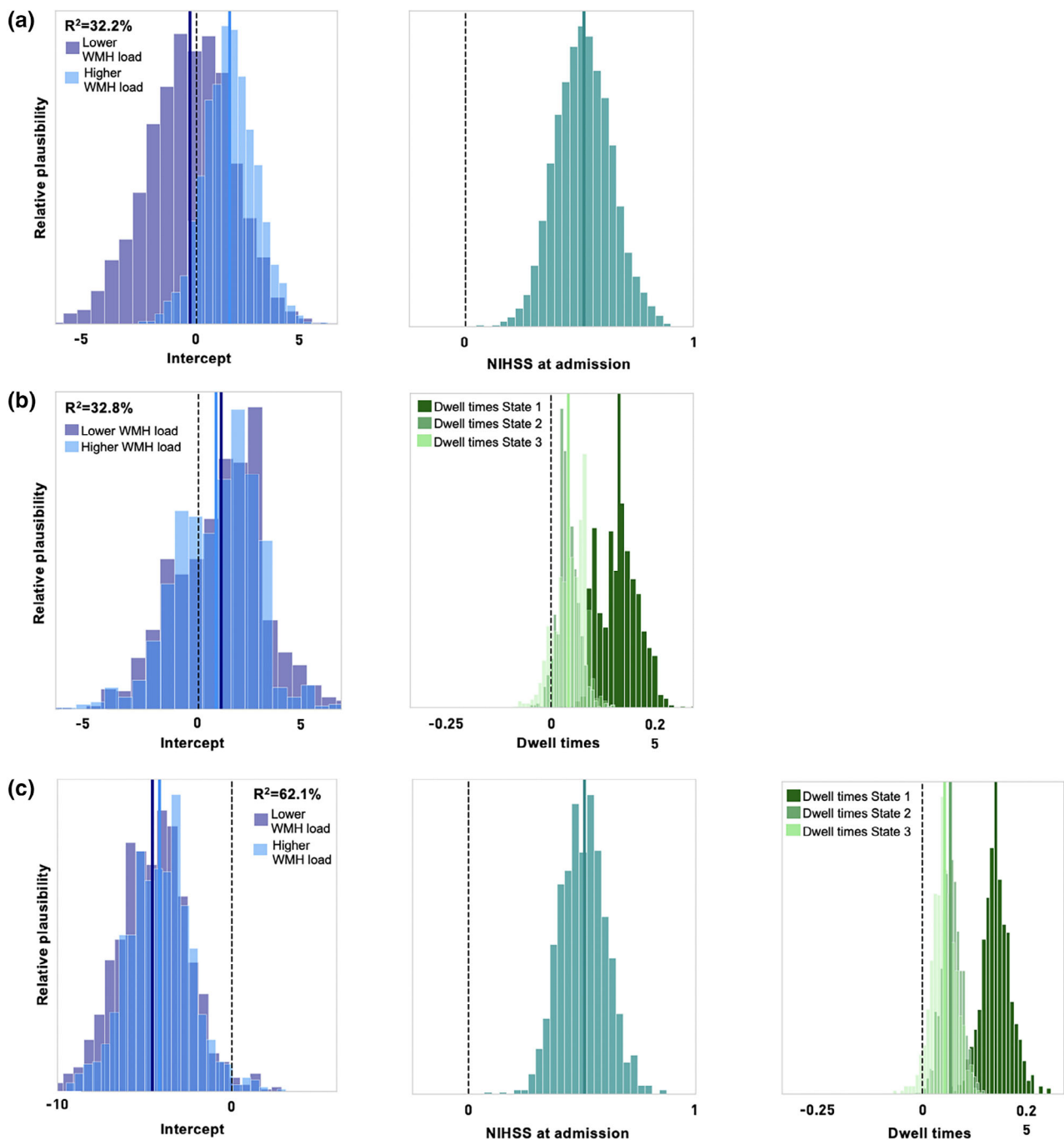


FIGURE 6 Bayesian hierarchical modeling of the stroke severity at time of scanning: Posterior parameter distributions. (a) Acute baseline model. The model based on the NIHSS score at admission, thus on average 3 days earlier, could predict the NIHSS at time of scanning with an explained variance of 32.3% (obtained via posterior predictive checks). The intercept for patients with a higher white matter hyperintensity load indicated a higher predicted NIHSS score at time of scanning (light blue) compared to the group of patients with a lower white matter hyperintensity load (dark blue). The parameter posterior mean of 0.51 for the NIHSS scores at admission denoted a decrease in NIHSS stroke severity until the time of scanning (right plot). (b) Acute dynamic model. A higher dwell time in any of the three states predicted a higher NIHSS score at the time of scanning, the explained variance was 32.8%. This effect was particularly strong for dwell times in State 1 (dark green). The effect of the white matter hyperintensity load on stroke severity did not differ between the groups of moderate and high white matter hyperintensity loads. (c) Acute extended model relying on the NIHSS at admission as well as the derived dwell times. A higher NIHSS score at admission, as well as higher dwell times, mainly in State 1, continued to be predictive of a higher NIHSS score at the time of scanning. Explained variance of the joint model was 62.1%

significantly more time in State 1 with highly positive intra- and highly negative inter-domain connectivity. This strong intra-domain connectivity was particularly apparent for the visual and sensorimotor

domains. In contrast, State 2, a weakly connected state, comprised rather low intra- and mostly neutral inter-domain connectivity. State 3 featured a combination of both previous states with positive intra-

domain connectivity and slightly positive inter-domain connectivity. While the times spent in State 2 and 3 did not differ significantly between patient groups, all three states comprised significantly altered dynamic connectivity between multiple brain areas.

4.1 | Segregation and acute stroke severity

Patients experiencing severe strokes had a significant predilection for the densely connected State 1. Since this state exhibited strong positive intra-network connectivity, brain areas belonging to the same functional domain, for example, the precentral and postcentral areas of the cortical sensorimotor domain, could easily exchange information. Conversely, the strong negative inter-network connectivity indicated a lower level of communication between different functional domains. This pattern of isolated information processing within functional domains can be interpreted as *functional segregation*. *Functional integration*, on the other hand, implies an effortless information transfer within and between functional domains (Eickhoff & Grefkes, 2011).

A comparable preference for a segregated state in case of more severe deficits has recently been described in an independent cohort of acute stroke patients, who presented with a comparable spectrum of symptom severity and were also scanned within the first days after their cerebrovascular events (Bonkhoff, Espinoza, et al., 2020). In this study, patients with severe motor impairments had a significantly higher probability of transitioning into a dynamic connectivity state that was characterized by a high segregation between motor domains. Paralleling these findings, a recent study described an increasing segregation between somatomotor systems due to cast-induced inactivity of the dominant upper limb in otherwise healthy adults (Newbold et al., 2020). Further nonstroke-related studies suggest an association between higher levels of segregation and larger gains in cognitive and motor skill learning in health (Mattar et al., 2018) and disease (Arnnemann et al., 2015). Nonetheless, we here did not find a significant correlation between the level of segregation and changes in stroke severity in the first 3 months poststroke. Therefore, the dynamic increase in segregation observed in our study primarily appeared as an expression of deteriorated, lost function, and not a mechanism supporting brain plasticity and recovery.

Neuropsychiatric diseases, such as schizophrenia, bipolar disorder or autism, have primarily been linked to increased times spent in weakly connected states, such as our State 2 (c.f., schizophrenia: Damaraju et al., 2014, bipolar disorder: Rashid, Damaraju, Pearson, & Calhoun, 2014, autism: Fu et al., 2019). This increased occurrence of less segregated states was suggested to represent reduced vigilance and enhanced self-focused thought (Allen et al., 2014; Marusak et al., 2017). On the other hand, many neurological diseases, for example, migraine, anti-NMDA-receptor encephalitis, Parkinson's disease and—as also presented here—stroke show the opposite pattern. Neurological patients apparently exhibit a preference for highly connected, segregated dynamic connectivity states, such as our State 1. This preference may thus

denote a joint signature of limited neurological function (c.f., migraine: Tu et al., 2019, anti-NMDA-receptor encephalitis: von Schwanenflug et al., 2020, Parkinson's disease: Kim et al., 2017, stroke: Bonkhoff, Espinoza, et al., 2020).

4.2 | Alterations in dynamic connectivity: Acute stroke severity

We detected wide-spread differences in dynamic connectivity between brain areas of various functional domains. These connectivity pairs were significantly altered between the three severity defined groups of stroke patients and also significantly correlated with stroke severity at time of scanning across the entirety of stroke patients. In particular, we noted the inter-hemispheric decrease in connectivity between cortical motor areas that is frequently reported in rsfMRI stroke studies focused on motor impairments (Carter et al., 2010; Golestani et al., 2013; Rehme et al., 2014; Wang et al., 2010). However, we ascertained this alteration between mildly and moderately affected patients only. We did not detect similar connectivity decreases between mildly and severely or moderately and severely affected patients, despite the prior expectation that more severe stroke symptoms would cause more extensive changes. A comparable discrepancy was also observed in a previous dFNC study in AIS patients (Bonkhoff, Espinoza, et al., 2020). Importantly, the initial descriptions of this specific connectivity decrease between bilateral motor areas were based on plain comparisons of stroke patients and controls (Carter et al., 2010; Golestani et al., 2013; Rehme et al., 2014; Wang et al., 2010). The exact amount of motor impairment was not considered and analyses therefore did not allow for more granular observations of links between connectivity strengths and symptom severity. Thus, future studies could aim to confirm and further elucidate the biological meaning of bilateral motor area connectivity in relation to stroke severity—for example, is it beneficial or detrimental in the process of stroke recovery?

4.3 | Alterations in dynamic connectivity: Recovery of stroke severity

Dynamic connectivity between three network pairs was either significantly correlated with the realized recovery in stroke severity in the first 3 months after stroke or showed strong trends. The densely connected State 1 comprised a significant negative correlation between the change in stroke severity and the dynamic connectivity of the default mode networks *bilateral intraparietal lobule* and *left angular gyrus*. Additionally, State 3 presented two positive correlations between recovery in stroke severity and the dynamic connectivity of *bilateral putamen* and *bilateral superior temporal gyrus*, as well as the same *putamen network* and *bilateral anterior insula*. Observed changes hence involved the subcortical motor, auditory, cognitive control, and default mode network domains. The revealed importance of the subcortical putamen connectivity for stroke outcome may primarily relate

to the recovery of motor symptoms that account for a substantial fraction of NIHSS points. With regard to the cognitive control and default mode networks: These domains are well known to encompass cortical hubs that are globally well-connected and essential to orchestrate various brain functions (Van Den Heuvel & Sporns, 2011). Recent stroke studies relying on structural MRI data already indicated worse stroke outcomes the more of such well-connected areas were affected by stroke lesions (Ktena et al., 2019; Schirmer et al., 2019). Previous functional MRI studies have also reported disturbed functional connectivity within the default mode network when comparing subacute ischemic stroke patients and healthy controls, independent of any specific, cognitive deficits or stroke severity (Ding et al., 2014; Tuladhar et al., 2013). While the extracted areas slightly differ between studies, likely due to varying outcome measures, group definitions and scanning time points, previous studies and ours combined suggest that cognitive control and default mode networks may play essential roles for stroke outcome and recovery in addition to motor-related domains.

4.4 | Modeling stroke severity

The individual dwell times, i.e., the time spent in all the three states without any interruption, proved to be equally effective in predicting the stroke severity at the time of scanning as the NIHSS score at the time of admission based on our Bayesian hierarchical models (Gelman & Hill, 2006). Moreover, the combination of dynamic connectivity measures and clinical information led to the highest prediction performance, as it was the highest-ranked model in the Bayesian model comparison. However, the maximum explained variance of 62% still leaves a substantial amount of the variance in recovery unexplained and might thus call for an even more comprehensive collection of outcome predictors (Bonkhoff et al., 2020). Our ancillary analysis already suggested an additionally relevant effect of age on the stroke severity. However, we did not detect any effects of sex or intravenous thrombolysis and did not have access to further clinical characteristics, such as perfusion deficits, the status of the collateral circulation, and the presence of large vessel occlusions, with probable predictive capacities.

Nonetheless, the increase in prediction performance based on our dynamic connectivity measures, as here observed, can be seen as evidence, that they represent information going beyond that of clinical measures. These dFNC measures may thus represent valid additional predictors of stroke outcome. This is yet a further demonstration of the potential utility of neuroimaging markers for the prediction of stroke symptoms. Previous studies have already begun to highlight the value of MRI derived measures. Examples of such predictors comprise the number of lesioned rich club regions, as obtained from structural MRI data (Schirmer et al., 2019). Lesion topographies as inferred from acute diffusion tensor imaging (Moulton, Valabregue, Lehericy, Samson, & Rosso, 2019), static connectivity between motor areas (Rehme et al., 2014), static whole-brain connectivity (Puig et al., 2018) and information on the network

topology (Ktena et al., 2019), as characterized by functional MRI data.

White matter disease has been associated with poorer early neurological outcomes after stroke in recent years (Etherton et al., 2019; Etherton, Wu, & Rost, 2016). We here investigated the differential effects of white matter hyperintensities on stroke severity by means of a hierarchical intercept term. In case of the admission-NIHSS model, group-wise intercepts diverged: In accordance with previous studies, a higher white matter hyperintensity lesion load was predictive of a higher stroke severity at the time of scanning. Importantly, this effect was independent of the initial admission stroke severity.

4.5 | Further limitations and future directions

While of relatively modest sample size ($n = 41$), this study is both unique to and yet comparable with other published stroke cohorts undergoing rsfMRI in the acute post-stroke recovery phase. It is unique in its approach of assessing acute alterations in dynamic connectivity exclusively within strata of variably affected stroke patients, without the direct comparison to a healthy control group. Rather, the group of mildly affected stroke patients represents a control group to more severely affected patients. Importantly, healthy controls and patients probably differ not only with respect to the AIS, but also their chronic brain health profiles, as for example expressed by WMH lesion loads. This circumstance can lead to potential confounds—that, on the other hand, can be alleviated when contrasting patient subgroups with conceivably more similar risk profiles. Furthermore, our dataset is comparable in size with prior dynamic functional connectivity studies in the first few days after stroke (Hu et al., 2018: 19 patients; Bonkhoff, Espinoza, et al., 2020: 31 patients; Bonkhoff, Rehme, et al., 2020: 54 patients). Notably, one of our main findings, that is, favored transiently increased segregation in case of a high stroke severity, is well in line with previous reports of increased transition likelihood to segregated states in case of severe motor impairments (Bonkhoff, Espinoza, et al., 2020). Altogether, this agreement demonstrates the overall robustness of results for these kinds of dataset sizes.

The reliability of dynamic analyses may be comparatively inferior to the one of static functional analyses (Zhang, Baum, Adduru, Biswal, & Michael, 2018) and it was suggested to increase the duration of scans beyond 10 min to allow for the exploration of *all* aspects of dynamic connectivity alterations (Hutchison et al., 2013). Hence, our relatively short current scan length of ~ 6 min can be considered a limitation of this study. However, we opted for this length to increase the clinical feasibility. Lastly, the aforementioned agreement between dynamic connectivity stroke studies may indicate that our scan length was sufficient for a stable derivation of dynamic connectivity.

Furthermore, previous research has identified more frequently occurring pronounced hemodynamic lags of resting-state signals in patients with cerebrovascular disease, that can have distorting effects on functional connectivity evaluations (Christen et al., 2015; Siegel, Snyder, Ramsey, Shulman, & Corbetta, 2016). In accordance with

recommendations by Siegel and colleagues on how to approach potential hemodynamic lags in stroke patients' rsfMRI data (Siegel, Shulman, & Corbetta, 2017), we here focused on ensuring the absence of severe and widespread time delays (i.e., no entire hemisphere was delayed by more than 1 s relative to the other hemisphere). In future investigations, our hemisphere-focused, spatially coarse-grained approach to time delay analyses could be rendered more spatially specific (Siegel et al., 2016; Tanrıtanır et al., 2020) and advanced methods to correct for time delays could be considered (Erdoğan et al., 2016; Jahanian, Christen, Moseley, & Zaharchuk, 2018).

Comparable to many previous stroke imaging studies (Salvalaggio, De Filippo De Grazia, Zorzi, Thiebaut de Schotten, & Corbetta, 2020; Stockert et al., 2020; Volz et al., 2016), our aim was to concurrently investigate direct, as well as indirect lesion effects, since both of them can lead to differences in behavior. Thus, we decided against the exclusion of lesioned brain regions in the dynamic functional connectivity analysis itself. Future studies could complement our approach by focusing on only indirect lesion effects and exclude brain regions affected by ischemia and perfusion deficits, as for example indicated by DWI-hyperintense lesions and rsfMRI-based hemodynamic delays.

In this study, we focused on stroke severity, measured on the NIHSS scale, as the main outcome of interest. The NIHSS can already be considered more granular than the frequently used modified Rankin Scale score. Given that the NIHSS ascribes high weights to motor and language impairments, the alterations seen here conceivable mostly relate to these impairment categories. Nonetheless, the unavailability of an even more fine-grained score that would capture specific impairments, for example, in the cognitive or language domains, can be seen as a current limitation. Especially in view of numerous insight-generating dFNC studies in the field of cognitive decline (e.g., subcortical ischemic vascular disease: Fu et al., 2019, Alzheimer's disease: de Vos et al., 2018), future studies are warranted to explore dynamic connectivity alterations in relation to these specific symptoms post-stroke further.

Finally, while stroke populations may generally have a higher load of WMH lesions (Rost et al., 2010), we embraced this characteristic even more explicitly by recruiting stroke patients with higher WMH lesions loads. This criterion may have had an effect on functional connectivity on its own, as previous literature suggests connectivity alterations based on white matter disease (Reijmer et al., 2015). However, we here did not find any significant correlations between the WMH lesion load and any of the dynamic connectivity estimates. We furthermore included the WMH lesion load in our Bayesian prediction models, which rendered their influence on stroke outcome apparent. Our approach may motivate a more frequent inclusion of WMH lesion load as proxy of chronic small vessel disease in future stroke imaging studies.

5 | CONCLUSION

We here revealed transiently increased isolated information processing of functional domains in severe stroke by leveraging

dynamic functional network connectivity analyses. Since we did not observe a correlation between this enhanced isolated information processing and the amount of recovery poststroke, this alteration was primarily interpretable as expression of deteriorated function. The change in stroke severity in the first 3 months poststroke was furthermore linked to dynamic connectivity involving default mode network components, suggesting a pivotal role of this domain in stroke recovery.

ACKNOWLEDGMENTS

We are grateful to our colleagues at the J. Philip Kistler Stroke Research Center for valuable support and discussions. Furthermore, we are grateful to our research participants without whom this work would not have been possible.

CONFLICT OF INTERESTS

Ona Wu has served as a consultant for Penumbra, Inc.; Advisory Board Member for Genentech, Inc. N. S. R. has received compensation as scientific advisory consultant from Omnix, Sanofi Genzyme and AbbVie Inc. The other authors report no relevant disclosures.

ETHICS STATEMENT

The study was approved by the institutional review board (Massachusetts General Hospital, Boston, MA) and all participants, or their surrogates, gave written informed consent at the time of study enrollment.

DATA AVAILABILITY STATEMENT

The authors agree to make the data available to any researcher for the express purposes of reproducing the here presented results and with the explicit permission for data sharing by the local institutional review board. Matlab and jupyter notebook scripts, that generated the presented results, will be made available on GitHub upon publication.

ORCID

Anna K. Bonkhoff  <https://orcid.org/0000-0002-5927-1089>

Christian Grefkes  <https://orcid.org/0000-0001-8007-9588>

REFERENCES

- Allen, E. A., Damaraju, E., Plis, S. M., Erhardt, E. B., Eichele, T., & Calhoun, V. D. (2014). Tracking whole-brain connectivity dynamics in the resting state. *Cerebral Cortex*, 24(3), 663–676. <https://doi.org/10.1093/cercor/bhs352>
- Arndemann, K. L., Chen, A. J.-W., Novakovic-Agopian, T., Gratton, C., Nomura, E. M., & D'Esposito, M. (2015). Functional brain network modularity predicts response to cognitive training after brain injury. *Neurology*, 84(15), 1568–1574.
- Ashburner, J., & Friston, K. J. (2005). Unified segmentation. *NeuroImage*, 26(3), 839–851.
- Bonkhoff, A. K., Espinoza, F. A., Gazula, H., Vergara, V. M., Hensel, L., Michely, J., ... Grefkes, C. (2020). Acute ischaemic stroke alters the brain's preference for distinct dynamic connectivity states. *Brain*, 143, 1525–1540. <https://doi.org/10.1093/brain/awaa101>

- Bonkhoff, A. K., Hope, T., Bzdok, D., Guggisberg, A. G., Hawe, R. L., Dukelow, S. P., ... Bowman, H. (2020). Bringing proportional recovery into proportion: Bayesian modelling of post-stroke motor impairment. *Brain*, 143, 2189–2206. <https://doi.org/10.1093/brain/awaa146>
- Bonkhoff, A. K., Rehme, A., Hensel, L., Tscherpel, C., Volz, L., Espinoza, F., ... Rost, N. (2020). Dynamic connectivity predicts acute motor impairment and recovery post-stroke. *medRxiv*.
- Brett, M., Leff, A. P., Rorden, C., & Ashburner, J. (2001). Spatial normalization of brain images with focal lesions using cost function masking. *NeuroImage*, 14(2), 486–500.
- Calhoun, V. D., Miller, R., Pearlson, G., & Adalı, T. (2014). The Chronnectome: Time-varying connectivity networks as the next frontier in fMRI data discovery. *Neuron*, 84(2), 262–274. <https://doi.org/10.1016/j.neuron.2014.10.015>
- Carter, A. R., Astafiev, S. V., Lang, C. E., Connor, L. T., Rengachary, J., Strube, M. J., ... Corbetta, M. (2010). Resting interhemispheric functional magnetic resonance imaging connectivity predicts performance after stroke. *Annals of Neurology*, 67(3), 365–375.
- Chang, C., & Glover, G. H. (2010). Time–frequency dynamics of resting-state brain connectivity measured with fMRI. *NeuroImage*, 50(1), 81–98.
- Christen, T., Jahanian, H., Ni, W. W., Qiu, D., Moseley, M. E., & Zaharchuk, G. (2015). Noncontrast mapping of arterial delay and functional connectivity using resting-state functional MRI: A study in Moyamoya patients. *Journal of Magnetic Resonance Imaging*, 41(2), 424–430. <https://doi.org/10.1002/jmri.24558>
- Collaborators, G. 2016 L. R. of S. (2018). Global, regional, and country-specific lifetime risks of stroke, 1990 and 2016. *New England Journal of Medicine*, 379(25), 2429–2437.
- Corbetta, M., Ramsey, L., Callejas, A., Baldassarre, A., Hacker, C. D., Siegel, J. S., ... Shulman, G. L. (2015). Common behavioral clusters and subcortical anatomy in stroke. *Neuron*, 85(5), 927–941. <https://doi.org/10.1016/j.neuron.2015.02.027>
- Damaraju, E., Allen, E. A., Belger, A., Ford, J. M., McEwen, S., Mathalon, D. H., ... Calhoun, V. D. (2014). Dynamic functional connectivity analysis reveals transient states of dysconnectivity in schizophrenia. *NeuroImage: Clinical*, 5, 298–308. <https://doi.org/10.1016/j.nicl.2014.07.003>
- de Vos, F., Koini, M., Schouten, T. M., Seiler, S., van der Grond, J., Lechner, A., ... Rombouts, S. A. R. B. (2018). A comprehensive analysis of resting state fMRI measures to classify individual patients with Alzheimer's disease. *NeuroImage*, 167, 62–72. <https://doi.org/10.1016/j.neuroimage.2017.11.025>
- Ding, X., Li, C.-Y., Wang, Q.-S., Du, F.-Z., Ke, Z.-W., Peng, F., ... Chen, L. (2014). Patterns in default-mode network connectivity for determining outcomes in cognitive function in acute stroke patients. *Neuroscience*, 277, 637–646. <https://doi.org/10.1016/j.neuroscience.2014.07.060>
- Du, Y., & Fan, Y. (2013). Group information guided ICA for fMRI data analysis. *NeuroImage*, 69, 157–197.
- Eickhoff, S. B., & Grefkes, C. (2011). Approaches for the integrated analysis of structure, function and connectivity of the human brain. *Clinical EEG and Neuroscience*, 42(2), 107–121.
- Erdoğan, S. B., Tong, Y., Hocke, L. M., Lindsey, K. P., & deB Frederick, B. (2016). Correcting for blood arrival time in global mean regression enhances functional connectivity analysis of resting state fMRI-BOLD signals. *Frontiers in Human Neuroscience*, 10, 311.
- Espinoza, F. A., Liu, J., Ciarochi, J., Turner, J. A., Vergara, V. M., Caprihan, A., ... Calhoun, V. D. (2019). Dynamic functional network connectivity in Huntington's disease and its associations with motor and cognitive measures. *Human Brain Mapping*, 40, 1955–1968. <https://doi.org/10.1002/hbm.24504>
- Espinoza, F. A., Turner, J. A., Vergara, V. M., Miller, R. L., Mennigen, E., Liu, J., ... Calhoun, V. D. (2018). Whole-brain connectivity in a large study of Huntington's disease gene mutation carriers and healthy controls. *Brain Connectivity*, 8(3), 166–178. <https://doi.org/10.1089/brain.2017.0538>
- Etherton, M. R., Wu, O., Giese, A.-K., Lauer, A., Boulouis, G., Mills, B., ... Schaefer, P. (2019). White matter integrity and early outcomes after acute ischemic stroke. *Translational Stroke Research*, 10(6), 630–638.
- Etherton, M. R., Wu, O., & Rost, N. S. (2016). Recent advances in Leukoaraiosis: White matter structural integrity and functional outcomes after acute ischemic stroke. *Current Cardiology Reports*, 18(12), 123. <https://doi.org/10.1007/s11886-016-0803-0>
- Fazekas, F., Chawluk, J. B., Alavi, A., Hurtig, H. I., & Zimmerman, R. A. (1987). MR signal abnormalities at 1.5 T in Alzheimer's dementia and normal aging. *American Journal of Roentgenology*, 149(2), 351–356.
- Fu, Z., Iraj, A., Caprihan, A., Adair, J. C., Sui, J., Rosenberg, G. A., & Calhoun, V. D. (2019). In search of multimodal brain alterations in Alzheimer's and Binswanger's disease. *NeuroImage: Clinical*, 26, 101937. <https://doi.org/10.1016/j.nicl.2019.101937>
- Fu, Z., Tu, Y., Di, X., Du, Y., Sui, J., Biswal, B. B., ... Calhoun, V. D. (2019). Transient increased thalamic-sensory connectivity and decreased whole-brain dynamism in autism. *NeuroImage*, 190, 191–204. <https://doi.org/10.1016/j.neuroimage.2018.06.003>
- Gelman, A., & Hill, J. (2006). *Data analysis using regression and multilevel/hierarchical models*. Cambridge, England: Cambridge University Press.
- Gibbs, N. M., & Gibbs, S. V. (2015). Misuse of 'trend' to describe 'almost significant' differences in anaesthesia research. *British Journal of Anaesthesia*, 115(3), 337–339. <https://doi.org/10.1093/bja/aev149>
- Golestani, A.-M., Tymchuk, S., Demchuk, A., Goodyear, B. G., & VISION-2 Study Group. (2013). Longitudinal evaluation of resting-state fMRI after acute stroke with hemiparesis. *Neurorehabilitation and Neural Repair*, 27(2), 153–163. <https://doi.org/10.1177/1545968312457827>
- Grefkes, C., & Fink, G. R. (2014). Connectivity-based approaches in stroke and recovery of function. *The Lancet Neurology*, 13(2), 206–216.
- Hu, J., Du, J., Xu, Q., Yang, F., Zeng, F., Weng, Y., ... Zhang, Z. (2018). Dynamic network analysis reveals altered temporal variability in brain regions after stroke: A longitudinal resting-state fMRI study. *Neural Plasticity*, 2018, 1–10. <https://doi.org/10.1155/2018/9394156>
- Hutchison, R. M., Womelsdorf, T., Allen, E. A., Bandettini, P. A., Calhoun, V. D., Corbetta, M., ... Chang, C. (2013). Dynamic functional connectivity: Promise, issues, and interpretations. *NeuroImage*, 80, 360–378. <https://doi.org/10.1016/j.neuroimage.2013.05.079>
- Jahanian, H., Christen, T., Moseley, M. E., & Zaharchuk, G. (2018). Erroneous resting-state fMRI connectivity maps due to prolonged arterial arrival time and how to fix them. *Brain Connectivity*, 8(6), 362–370. <https://doi.org/10.1089/brain.2018.0610>
- Kim, J., Criaud, M., Cho, S. S., Díez-Cirarda, M., Mihaescu, A., Coakeley, S., ... Houle, S. (2017). Abnormal intrinsic brain functional network dynamics in Parkinson's disease. *Brain*, 140(11), 2955–2967.
- Ktena, S. I., Schirmer, M. D., Etherton, M. R., Giese, A.-K., Tuozzo, C., Mills, B. B., ... Rost, N. S. (2019). Brain connectivity measures improve modeling of functional outcome after acute ischemic stroke. *Stroke*, 50(10), 2761–2767.
- Lassalle-Lagade, S., Sibon, I., Dilharreguy, B., Renou, P., Fleury, O., & Allard, M. (2012). Subacute default mode network dysfunction in the prediction of post-stroke depression severity. *Radiology*, 264(1), 218–224. <https://doi.org/10.1148/radiol.12111718>
- Lin, D. J., Cloutier, A. M., Erler, K. S., Cassidy, J. M., Snider, S. B., Ranford, J., ... Schwamm, L. H. (2019). Corticospinal tract injury estimated from acute stroke imaging predicts upper extremity motor recovery after stroke. *Stroke*, 50(12), 3569–3577.
- Lloyd, S. (1982). Least squares quantization in PCM. *IEEE Transactions on Information Theory*, 28(2), 129–137.
- Marusak, H. A., Calhoun, V. D., Brown, S., Crespo, L. M., Sala-Hamrick, K., Gotlib, I. H., & Thomason, M. E. (2017). Dynamic functional connectivity of neurocognitive networks in children. *Human Brain Mapping*, 38(1), 97–108.

- Mattar, M. G., Wymbs, N. F., Bock, A. S., Aguirre, G. K., Grafton, S. T., & Basset, D. S. (2018). Predicting future learning from baseline network architecture. *NeuroImage*, 172, 107–117.
- Moulton, E., Valabregue, R., Lehericy, S., Samson, Y., & Rosso, C. (2019). Multivariate prediction of functional outcome using lesion topography characterized by acute diffusion tensor imaging. *NeuroImage: Clinical*, 23, 101821.
- Newbold, D. J., Laumann, T. O., Hoyt, C. R., Hampton, J. M., Montez, D. F., Raut, R. V., ... Dosenbach, N. U. F. (2020). Plasticity and spontaneous activity pulses in disused human brain circuits. *Neuron*, 107, 580–589. e6. <https://doi.org/10.1016/j.neuron.2020.05.007>
- Power, J. D., Schlaggar, B. L., & Petersen, S. E. (2015). Recent progress and outstanding issues in motion correction in resting state fMRI. *NeuroImage*, 105, 536–551. <https://doi.org/10.1016/j.neuroimage.2014.10.044>
- Puig, J., Blasco, G., Alberich-Bayarri, A., Schlaug, G., Deco, G., Biarnes, C., ... Pedraza, S. (2018). Resting-state functional connectivity magnetic resonance imaging and outcome after acute stroke. *Stroke*, 49(10), 2353–2360. <https://doi.org/10.1161/STROKEAHA.118.021319>
- Rashid, B., Damaraju, E., Pearlson, G. D., & Calhoun, V. D. (2014). Dynamic connectivity states estimated from resting fMRI identify differences among schizophrenia, bipolar disorder, and healthy control subjects. *Frontiers in Human Neuroscience*, 8, 897.
- Rehme, A. K., Volz, L. J., Feis, D.-L., Bomilcar-Focke, I., Liebig, T., Eickhoff, S. B., ... Grefkes, C. (2014). Identifying neuroimaging markers of motor disability in acute stroke by machine learning techniques. *Cerebral Cortex*, 25(9), 3046–3056.
- Reijmer, Y. D., Schultz, A. P., Leemans, A., O'sullivan, M. J., Gurol, M. E., Sperling, R., ... Hedden, T. (2015). Decoupling of structural and functional brain connectivity in older adults with white matter hyperintensities. *NeuroImage*, 117, 222–229.
- Rost, N. S., Fitzpatrick, K., Biffi, A., Kanakis, A., Devan, W., Anderson, C. D., ... Rosand, J. (2010). White matter hyperintensity burden and susceptibility to cerebral ischemia. *Stroke*, 41(12), 2807–2811. <https://doi.org/10.1161/STROKEAHA.110.595355>
- Salman, M. S., Du, Y., Lin, D., Fu, Z., Fedorov, A., Damaraju, E., ... Posse, S. (2019). Group ICA for identifying biomarkers in schizophrenia: 'Adaptive' networks via spatially constrained ICA show more sensitivity to group differences than spatio-temporal regression. *NeuroImage: Clinical*, 22, 101747.
- Salvalaggio, A., De Filippo De Grazia, M., Zorzi, M., Thiebaut de Schotten, M., & Corbetta, M. (2020). Post-stroke deficit prediction from lesion and indirect structural and functional disconnection. *Brain*, 143(7), 2173–2188. <https://doi.org/10.1093/brain/awaa156>
- Salvatier, J., Wiecki, T. V., & Fonnesbeck, C. (2016). Probabilistic programming in python using PyMC3. *PeerJ Computer Science*, 2, e55.
- Schirmer, M. D., Ktena, S. I., Nardin, M. J., Donahue, K. L., Giese, A.-K., Etherton, M. R., ... Rost, N. S. (2019). Rich-club organization: An important determinant of functional outcome after acute ischemic stroke. *Frontiers in Neurology*, 10, 956. <https://doi.org/10.3389/fneur.2019.00956>
- Siegel, J. S., Shulman, G. L., & Corbetta, M. (2017). Measuring functional connectivity in stroke: Approaches and considerations. *Journal of Cerebral Blood Flow & Metabolism*, 37(8), 2665–2678. <https://doi.org/10.1177/0271678X17709198>
- Siegel, J. S., Snyder, A. Z., Ramsey, L., Shulman, G. L., & Corbetta, M. (2016). The effects of hemodynamic lag on functional connectivity and behavior after stroke. *Journal of Cerebral Blood Flow & Metabolism*, 36(12), 2162–2176. <https://doi.org/10.1177/0271678X15614846>
- Stockert, A., Wawrzyniak, M., Klingbeil, J., Wrede, K., Kümmerer, D., Hartwigsen, G., ... Saur, D. (2020). Dynamics of language reorganization after left temporo-parietal and frontal stroke. *Brain*, 143(3), 844–861. <https://doi.org/10.1093/brain/awaa023>
- Tanntanir, A. C., Villringer, K., Galinovic, I., Grittner, U., Kirilina, E., Fiebach, J. B., ... Khalil, A. A. (2020). The effect of scan length on the assessment of BOLD delay in ischemic stroke. *Frontiers in Neurology*, 11, 381.
- Tu, Y., Fu, Z., Zeng, F., Maleki, N., Lan, L., Li, Z., ... Liu, M. (2019). Abnormal thalamocortical network dynamics in migraine. *Neurology*, 92(23), e2706–e2716.
- Tuladhar, A. M., Snaphaan, L., Shumskaya, E., Rijpkema, M., Fernandez, G., Norris, D. G., & de Leeuw, F.-E. (2013). Default mode network connectivity in stroke patients. *PLoS One*, 8(6), e66556. <https://doi.org/10.1371/journal.pone.0066556>
- Van Den Heuvel, M. P., & Sporns, O. (2011). Rich-club organization of the human connectome. *Journal of Neuroscience*, 31(44), 15775–15786.
- Varoquaux, G., Gramfort, A., Poline, J.-B., & Thirion, B. (2010). Brain covariance selection: Better individual functional connectivity models using population prior. *Advances in Neural Information Processing Systems*, 2334–2342.
- Vidaurre, D., Arenas, A. L., Smith, S. M., & Woolrich, M. W. (2019). Behavioural relevance of spontaneous, transient brain network interactions in fMRI. *NeuroImage*, 779736.
- Volz, L. J., Rehme, A. K., Michely, J., Nettekoven, C., Eickhoff, S. B., Fink, G. R., & Grefkes, C. (2016). Shaping early reorganization of neural networks promotes motor function after stroke. *Cerebral Cortex*, 26(6), 2882–2894.
- von Schwanenflug, N., Krohn, S., Heine, J., Paul, F., Prüss, H., & Finke, C. (2020). State-dependent signatures of Anti-NMDA-Receptor Encephalitis: A dynamic functional connectivity study. *Neuroscience*. <https://doi.org/10.1101/2020.06.12.141945>
- Wang, L., Yu, C., Chen, H., Qin, W., He, Y., Fan, F., ... Zang, Y. (2010). Dynamic functional reorganization of the motor execution network after stroke. *Brain*, 133(4), 1224–1238.
- Ward, N. S. (2017). Restoring brain function after stroke—Bridging the gap between animals and humans. *Nature Reviews Neurology*, 13(4), 244–255.
- Wood, J., Freemantle, N., King, M., & Nazareth, I. (2014). Trap of trends to statistical significance: Likelihood of near significant P value becoming more significant with extra data. *BMJ*, 348(mar31 2), g2215–g2215. <https://doi.org/10.1136/bmj.g2215>
- Zhang, C., Baum, S. A., Adduru, V. R., Biswal, B. B., & Michael, A. M. (2018). Test-retest reliability of dynamic functional connectivity in resting state fMRI. *NeuroImage*, 183, 907–918. <https://doi.org/10.1016/j.neuroimage.2018.08.021>

SUPPORTING INFORMATION

Additional supporting information may be found online in the Supporting Information section at the end of this article.

How to cite this article: Bonkhoff AK, Schirmer MD, Bretzner M, et al. Abnormal dynamic functional connectivity is linked to recovery after acute ischemic stroke. *Hum Brain Mapp*. 2021;42:2278–2291. <https://doi.org/10.1002/hbm.25366>